ROYAL SOCIETY
OF CHEMISTRY

COMMUNICATION

Check for updates

Aerosol deposition of porous metal–organic materials onto diverse solid supports†

Christine M. Montone and Eric D. Bloch ID *

This study introduces a novel method for creating surface coatings from porous materials, specifically metal–organic frameworks (MOFs) and porous coordination cages (PCCs). Employing a cost-effective medical nebulizer, we aerosolize MOF and cage particles onto diverse surfaces. The method's versatility is demonstrated by successful coating of various materials, including mixed MOF constituents. Characterization analyses confirm material integrity and stability, highlighting its potential for practical applications. The technique offers a rapid and reproducible means of generating uniform coatings with controlled properties, addressing challenges in scalability and stability associated with these advanced materials. This novel approach holds promise for diverse applications in environmental, industrial, and technological contexts.

Hybrid metal–organic materials, such as metal–organic frameworks (MOFs) and porous coordination cages (PCCs; cages; or metal–organic polyhedra-MOPs) offer distinct opportunities as advanced adsorptive materials.[1] These innovative solids have garnered significant attention due to their exceptional tunability,[2] high surface areas,[3] and diverse chemical functionality.[4] Both MOFs and cages offer a unique platform for tailoring structural features at the molecular level as a means to optimize for various applications,[5] particularly adsorptive processes.[6]

The precisely engineered pores within these materials facilitate the selective adsorption of gases and vapors,[7,8] making them desirable for addressing environmental and industrial challenges.[9] The incorporation of functional groups onto their surfaces enhances their affinity for target molecules,[10] enabling tailor-made adsorption. However, as the implementation of MOFs and cages advances, several challenges emerge. These include issues related to stability, scalability, reproducibility, and utilization. Other challenges notwithstanding, large-scale

implementation of these materials relies on any one of several processing approaches where pelletization,[11] incorporation into membranes,[12] or deposition onto surfaces may offer a benefit.[13] The immobilization of these porous materials onto or into a porous support requires careful consideration of factors such as material compatibility, loading efficiency, and preservation of adsorptive properties. Achieving a seamless integration of MOFs and PCCs with surfaces is a complex task that demands new synthetic strategies and robust characterization techniques.[14] This integration is an appealing target in the pursuit of MOF and PCC-based sensors and microelectronics.

Current strategies for the deposition of MOFs or cages onto surfaces encompass a range of techniques that seek to ensure a controlled and stable interface between the material and substrate. Vapor deposition methods,[15] including thermal evaporation and molecular layer deposition enable the direct growth of films on surfaces with precise control over thickness and composition.[16,17] Solution-based methods such as layer-by-layer assembly and electrochemical methods encompass direct synthetic routes where material is grown on a surface *via* reaction of metal and ligand precursors.[18,19] Additionally, post-synthetic methods may be used where particles are drop-cast onto surfaces or reacted with an anchoring group that allows their attachment to surfaces *via* covalent or non-covalent interactions.[20] Many of these strategies, however, are not broadly translatable across diverse structure or material types and are limited for certain porous solids. To address this, we have developed a rapid and straightforward approach to aerosolize appropriately sized MOF or cage particles onto a broad range of surfaces. Here we show that a cheap medical grade nebulizer can be used to deposit MOF and cage particles onto different substrates.

To establish a versatile and practical method for creating surface coatings from a range of porous materials (Fig. 1), we initially experimented with a drop casting technique. We prepared both a methanol-soluble cage, $[Zr_{12}(\mu_3\text{-O})_4(\mu_2\text{-OH})_{12}(Cp)_{12}(m\text{-bdc})_6]Cl_4$ (Cp- = cyclopentadiene; m-bdc2- = isophthalate) and an insoluble cage, $Cu_{24}(5\text{-undecoxy-bdc})_{24}$, in

Department of Chemistry, Indiana University, Bloomington, Indiana 47405, USA.
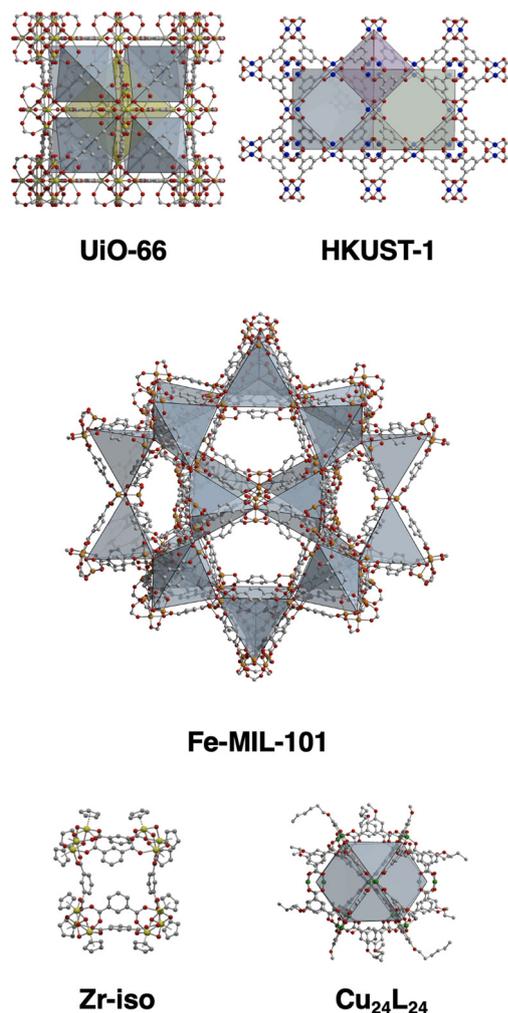*E-mail: edbloch@iu.edu*

Fig. 1 Structures of the MOFs and cages used in this study where the insoluble MOFs UiO-66, HKUST-1, and MIL-101 are compared to soluble cage Zr-iso and insoluble cage $Cu_{24}(undecoxy-bdc)_{24}$.

methanol, which were subsequently drop cast onto carbon paper at a concentration of 10 mg mL^{-1}. Each application was followed by solvent evaporation, and the process was repeated 10 times. However, this approach resulted in sparse and uneven coatings on the substrate, rendering them unsuitable for further applications (Fig. 2 and 4). Subsequently, we transitioned to aerosol deposition
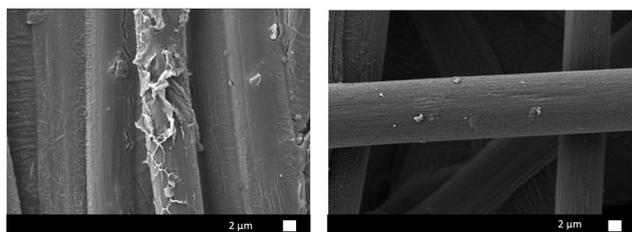

Fig. 2 SEM images of (left) $[Zr_{12}(\mu_3-O)_4(\mu_2-OH)_{12}(Cp)_{12}(m-bdc)_6]Cl_4$ dissolved in methanol then applied dropwise to carbon paper and (right) $Cu_{24}(5-undecoxy-bdc)_{24}$ suspended in methanol then applied dropwise to carbon paper. Note the near complete lack of surface deposition.

using an affordable medical nebulizer. For this particular nebulizer, its components were compatible with methanol, ethanol, and water as solvents. Given that methanol provided solubility for various cages, offered broad compatibility with other porous materials, and possessed the lowest boiling point among the three options, it emerged as the solvent of choice for this technique.

We commenced by exploring the aerosolization of the methanol-soluble cage, $[Zr_{12}(\mu_3-O)_4(\mu_2-OH)_{12}(Cp)_{12}(m-bdc)_6]Cl_4$ (hereafter referred to as Zr-iso). This material exhibited high solubility in methanol and was aerosolized as a solution onto a variety of substrates: carbon paper, nickel foam, zinc foil, molybdenum foil, and iron foil. Employing IR spectroscopy, PXRD, and SEM imaging, we characterized the resulting surface coatings. While IR spectra and PXRD patterns indicated the maintenance of chemical identity post-aerosolization, SEM images showcased a diverse array of particle sizes and morphologies (refer to Fig. 2). On certain surfaces, we observed the presence of semi-crystalline particles with diameters ranging from 1 to 10 micrometers. In contrast, other areas displayed morphologies like collapsed spheres or substantial aggregates of smaller nanoparticles. This variety of morphologies was influenced by the specific solvent evaporation conditions during each aerosolization trial. Despite using the same initial cage solution in methanol for each trial, the rate of solvent evaporation and particle formation varied due to the distinct properties of the substrates. Because the morphology and particle size is controlled by the crystallization process on each substrate, any variations in substrate surface texture, thermal conductivity, surface wetting, or other factors can greatly influence the nucleation and growth of particles. For example, the thermal conductivity of carbon paper is less than that of metal foils. Because of this, the solvent evaporation was likely slower on this substrate, leading to a wide distribution of collapsed spherical particles that formed from aerosolized droplets of cage solution slowly drying after being deposited on the surface. As can be seen in SEM images in Fig. S13–S15 (ESI†), the surface roughness/texture seemingly directs the nucleation of this material, resulting in different morphologies and distributions on each surface. This resulting inconsistency in particle morphology was not optimal and lacked reliable reproducibility across trials. This is not entirely unexpected when using a nebulizer to disperse a solution onto a support, whether porous or not, it deposits as a solution and particle formation or crystallization will proceed in the same manner as the solution drop-casting method. As a step towards achieving more uniform and predictable surface coatings, we explored different porous materials, particularly insoluble phases.

We reasoned that suspensions of cage or MOF would deposit in a more uniform manner during nebulizer-facilitated aerosolization, we turned to insoluble MOFs and cages. Reexamining the methanol-insoluble and MOF-like cage that showed poor compatibility with drop-casting, we prepared ~100 nm nanoparticles of $Cu_{24}(5-undecoxy-bdc)_{24}$. Notably, it remains insoluble in solvents suitable for the aerosolization process, including methanol. Methanol suspension was ideal for this process due to the relatively low boiling point and high

volatility, but importantly was also compatible with the plastic nebulizer components. This allows for an efficient deposition process where solvent evaporation was rapid and condensation of large droplets was avoided. In this way we were able to deposit the maximum amount of particles on each substrate without needing to heat the system to high temperatures, have high purge/drying gas flow through the system, or to waste large amounts of cage suspension. A concentration of 10 mg mL^{-1} of cage suspension was found to be ideal for this process-depositing a robust coating of particles without clogging the nebulizer components. We aerosolized Cu_{24}(5-undecoxy-bdc)$_{24}$ onto a range of substrates and subjected it to characterization through IR, PXRD, and SEM imaging. Both IR and PXRD analyses (Fig. S4 and S7 (ESI†), respectively) confirmed that the cage material retained its integrity after the aerosolization process, though PXRD demonstrates broadened peaks due to the small size of the particles. Furthermore, SEM imaging (Fig. S17–S21, ESI†) revealed that the particle size and morphology remained unchanged from the initially synthesized material. This outcome stood in stark contrast to the aerosolization of a solution containing a methanol-soluble cage, where particle size and morphology exhibited significant variation between different trials and surfaces.

We subsequently aimed to broaden the method's applicability to encompass MOFs, given their universal insolubility. We opted for widely studied and highly-stable UiO-66, a material we have previously demonstrated to adopt a range of nanoparticle sizes and diverse physical properties such as surface area and defectiveness.[21] Our prior work enabled efficient control of UiO-66 particle size by adjusting the ligand-to-metal ratio and the water content of the synthesis conditions. For this study, we selected three nanoparticle sizes spanning diameters from 34 to 72 nm. The smaller particle sizes proved particularly suitable for the aerosolization method and could uniformly coat an assortment of surfaces, even those that were uneven or rough, such as carbon paper. Fig. 3 and 4 show the SEM images depicting UiO-66 aerosolized onto carbon paper and additional substrates, revealing a dense and regular distribution of nanoparticles. Once again, IR and PXRD analyses (Fig. 3) played a pivotal role in confirming the deposited material's integrity post-aerosolization. Though the PXRD patterns for both the zirconium and copper-based cages (Fig. S6 and S7, ESI†) indicate largely amorphous materials for both bulk and aerosolized materials, the limited number of peaks were able to be matched from surface to surface. Pairing this with IR analysis of the fingerprint region allows for confirmation of the identity of the cage material deposited on each substrate. PXRD patterns for UiO-66 (Fig. S10, ESI†) reveal sharper peaks at 7° and 9° that were key features used to confirm the successful deposition of this MOF on each surface, as well as consistent IR spectra for each substrate (Fig. S5, ESI†).

Employing a more porous material enabled us to delve into the adsorption properties of post-aerosolized material, allowing for a comparison with the as-synthesized counterpart. To achieve this, we harnessed a thermogravimetric analysis (TGA) gas cycling method. Initially, 35 nm UiO-66 nanoparticles were aerosolized onto a heated glass surface, subsequently scraped off, and then transferred into an aluminum thermogravimetric analysis pan.
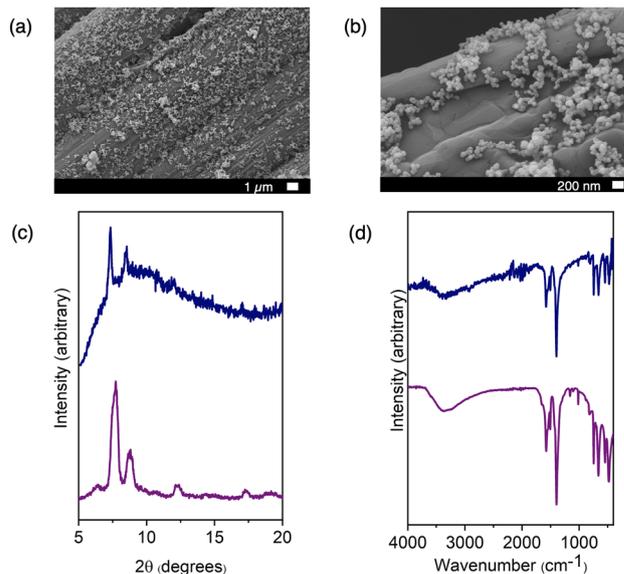

Fig. 3 Aerosolized UiO-66 nanoparticles deposited on carbon paper. (a) and (b) SEM images of particles at 10 000× and 50 000× magnification respectively. (c) Stacked PXRD pattern of material on carbon paper (blue) compared to bulk powder (purple). (d) Stacked IR spectra of material on carbon paper (blue) compared to bulk powder (purple). Spectra match in fingerprint region, indicating similarity of chemical species between bulk and deposited materials.

The sample underwent activation by heating to 100 °C within the TGA instrument under an N_2 atmosphere. Following this, the sample was cooled to 40 °C and dosed with 100% CO_2 for a duration of 10 minutes. These two gases were subjected to repeated isothermal cycling over 10 cycles. To establish a reference, an analogous sample of UiO-66 bulk material underwent a similar analysis, accompanied by a typical CO_2 isotherm executed at 40 °C, thereby enabling a comparison between the TGA method and conventional gas adsorption experiments. Notably, due to the limited quantity of aerosolized UiO-66 obtainable through repeated deposition and scraping, the TGA method was exclusively employed for this particular sample. Results from these three adsorption assessments exhibited favorable agreement between the aerosolized and bulk isotherms. This alignment indicates that the TGA cycling experiment serves as a commendable alternative to conventional isotherm experiments, particularly in scenarios where sample quantity is constrained. Crucially, these experiments underscore that the aerosolization method does not adversely impact the material's porosity. The material input is effectively retained after deposition, preserving its essential characteristics.

The aerosol coatings generally displayed high mechanical stability throughout the course of synthesis, activation, and characterization. To further assess this, we coated samples of carbon paper with either ∼100 nm Cu_{24}(5-undecoxy-bdc)$_{24}$ nanoparticles or ∼35 nm UiO-66 nanoparticles, which were immersed in methanol. Following immersion, the samples underwent sonication for durations of either 30 seconds or 5 minutes. Subsequently, the materials were carefully removed, subjected to drying, and imaged using SEM. Remarkably, the nanoparticles remained visible even after sonication, with an
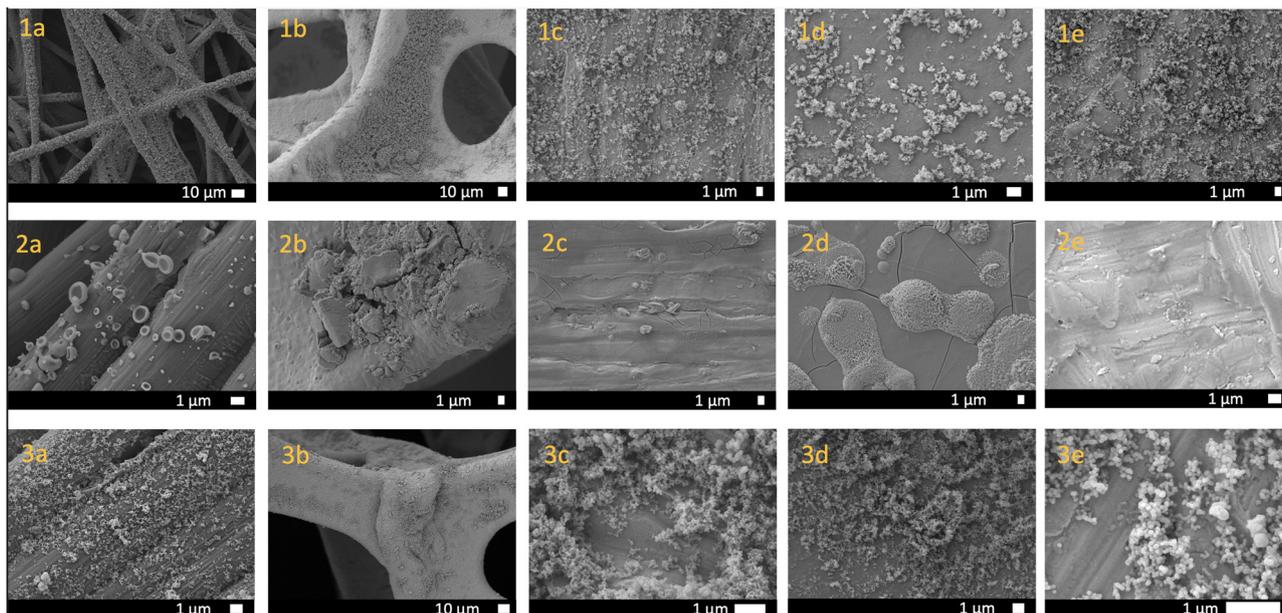
Fig. 4 SEM images for $Cu_{24}(5\text{-undecoxy-bdc})_{24}$ (#1), $[Zr_{12}(\mu_3\text{-O})_4(\mu_2\text{-OH})_{12}(Cp)_{12}(m\text{-bdc})_6]Cl_4$ (#2), and UiO-66 (#3) deposited onto carbon paper (a), nickel foam (b), molybdenum foil (c), iron foil (d), or zinc foil (e).

evident and consistent coating observed. Most notably, the particle morphology exhibited no discernible change. While this method strictly entails physical deposition, the interface between the substrate and particles demonstrated remarkable stability. This resilience resulted in a sustained uniform coating, effectively persevering across a range of substrates.

Lastly, we undertook an investigation into mixed MOF coatings. Initial attempts involved crystalline HKUST-1 and UiO-66 nanoparticles. We endeavored to aerosolize a suspension of this MOF mixture onto carbon paper. However, the outcome yielded a heterogeneous coating on the carbon paper's surface, primarily featuring a thick layer of UiO-66 and sporadic HKUST-1 particles. This outcome led us to recognize a limitation related to the nebulizer's size capacity. In response, we embarked on assessing various other MOF materials for compatibility with size constraints. Eventually, we opted for Fe-MIL-101 to be aerosolized alongside UiO-66. Employing energy dispersive X-ray analysis in tandem with SEM, we mapped the carbon paper's surface subsequent to the aerosol deposition of UiO-66 and Fe-MIL-101. The resultant elemental map unequivocally revealed a uniform coating of both zirconium and iron. This confirmation effectively signaled the successful coating of mixed MOF materials, underscoring the method's capability to create well-blended coatings even with diverse MOF constituents.

In conclusion, hybrid metal–organic materials, particularly metal–organic frameworks (MOFs) and porous coordination cages (PCCs), present promising opportunities as advanced adsorptive materials due to their tunability, high surface areas, and versatile chemical functionality. These materials offer a molecular-level structural tailoring platform, particularly suitable for optimizing adsorptive processes through precisely engineered pores that enable selective gas and vapor adsorption.

However, challenges such as stability, scalability, and reproducibility persist as these materials move toward practical implementation. To address these challenges, we introduced a rapid and straightforward approach for aerosolizing appropriately sized MOFs or cage particles onto diverse surfaces using a low-cost medical nebulizer. This technique was extensively investigated across different materials, leading to valuable insights. The method showcased distinct advantages in terms of particle morphology, stability, and uniformity on various substrates. Additionally, it demonstrated compatibility with mixed MOF coatings. Overall, this approach offers a versatile and promising avenue for creating well-defined surface coatings of porous materials, with potential applications spanning environmental, industrial, and technological domains.

Conflicts of interest

There are no conflicts to declare.

References

1 M. M. Deegan, A. M. Antonio, G. A. Taggart and E. D. Bloch, *Coord. Chem. Rev.*, 2021, **430**, 213679.
2 A. M. Antonio, K. J. Korman, M. M. Deegan, G. A. Taggart, G. P. A. Yap and E. D. Bloch, *Inorg. Chem.*, 2022, **61**, 4609–4617.

3 O. K. Farha, I. Eryazici, N. C. Jeong, B. G. Hauser, C. E. Wilmer, A. A. Sarjeant, R. Q. Snurr, S. T. Nguyen, A. Ö. Yazaydin and J. T. Hupp, *J. Am. Chem. Soc.*, 2012, **134**, 15016–15021.

4 G. E. Cmarik, M. Kim, S. M. Cohen and K. S. Walton, *Langmuir*, 2012, **28**, 15606–15613.

5 P. Gimeno-Fonquernie, W. Liang, J. Albalad, A. Kuznicki, J. R. Price, E. D. Bloch, C. J. Doonan and C. J. Sumby, *Chem. Commun.*, 2022, **58**, 957.

6 A. Kuznicki, G. R. Lorzing and E. D. Bloch, *Chem. Commun.*, 2021, **57**, 8312–8315.

7 O. T. Qazvini, R. Babarao and S. G. Telfer, *Nat. Commun.*, 2021, **12**, 197.

8 Y. Zhang, L. Gao, S. Ma and T. Hu, *J. Mater. Chem. C*, 2022, **10**, 1136–1143.

9 H. Kaur, M. Venkateswarulu, S. Kumar, V. Krishnan and R. R. Koner, *Dalton Trans.*, 2018, **47**, 1488–1497.

10 R. Cosialls, C. Simó, S. Borrós, V. Gómez-Vallejo, C. Schmidt, J. Llop, A. B. Cuenca and A. Casini, *Chem. – Eur. J.*, 2022, **29**, 3.

11 F. Lorignon, A. Gossard and M. Carboni, *Chem. Eng. J.*, 2020, **393**, 124765.

12 W. Li, P. Su, Z. Li, Z. Xu, F. Wang, H. Ou, J. Zhang, G. Zhang and E. Zeng, *Nat. Commun.*, 2017, **8**, 406.

13 L. D. Salmi, M. J. Heikkila, E. Puukilainen, T. Sajavaara, D. Grosso and M. Ritala, *Microporous Mesoporous Mater.*, 2013, **182**, 147–154.

14 L. Meng, B. Yu and Y. Qin, *Commun. Chem.*, 2021, **4**, 82.

15 F. J. Claire, M. A. Solomos, J. Kim, G. Wang, M. A. Siegler, M. F. Crommie and T. J. Kempa, *Nat. Commun.*, 2020, **11**, 5524.

16 A. M. Beiler, B. D. McCarthy, B. A. Johnson and S. Ott, *Nat. Commun.*, 2020, **11**, 5819.

17 A. L. Semrau, Z. Zhou, S. Mukherjee, M. Tu, W. Li and R. A. Fischer, *Langmuir*, 2021, **37**, 6847–6863.

18 V. Chernikova, O. Shekhah and M. Eddaoudi, *ACS Appl. Mater. Interfaces*, 2016, **8**, 20459–20464.

19 W. Wu, G. E. Decker, A. E. Weaver, A. I. Arnoff, E. D. Bloch and J. Rosenthal, *ACS Cent. Sci.*, 2021, **8**, 1427–1433.

20 N. K. Shrestha, S. A. Patil, S. Cho, Y. Jo, H. Kim and H. Im, *J. Mater. Chem. A*, 2020, **8**, 24408–24418.

21 G. E. Decker, Z. Stillman, L. Attia, C. A. Fromen and E. D. Bloch, *Chem. Mater.*, 2019, **31**, 4831–4839.